

Article

A Facile Strategy for the Ion Current and Fluorescence Dual-Lock in Detection: Naphthalic Anhydride Azide (NAA)-Modified Biomimetic Nanochannel Sensor towards H₂S

I Wu, Dan Zhang * and Xuanjun Zhang *

Faculty of Health Sciences, University of Macau, Macau 999078, China; yc17615@umac.mo

* Correspondence: yb97663@um.edu.mo (D.Z.); xuanjunzhang@um.edu.mo (X.Z.)

Abstract: Inspired by biological channels, the electric signal-based artificial nanochannel system exhibits high sensitivity in various analyses. However, ion current may be affected by many other factors, leading to false-positive signals. For reliable detection, in this work, we apply a facile strategy to combine both current signal and fluorescence. Fluorescent probes were conjugated to the nanochannel surface by covalent bonds. By utilizing the specific reduction of azide groups in the probe to amino groups by H₂S, a synchronizing change in fluorescence and nanochannel surface charge was established. As a result, both transmembrane ion current and fluorescence intensity showed significant changes. The photoelectric double-checked locking from temporal and spatial variation validly confirmed the response process and protected detection accuracy. The work may provide new ideas for the development of more sophisticated current and fluorescence dual-index nanochannel systems.



Citation: Wu, I.; Zhang, D.; Zhang, X. A Facile Strategy for the Ion Current and Fluorescence Dual-Lock in Detection: Naphthalic Anhydride Azide (NAA)-Modified Biomimetic Nanochannel Sensor towards H₂S. *Chemosensors* **2021**, *9*, 298. <https://doi.org/10.3390/chemosensors9110298>

Academic Editor:
Nicole Jaffrezic-Renault

Received: 16 August 2021
Accepted: 27 September 2021
Published: 24 October 2021

Publisher's Note: MDPI stays neutral with regard to jurisdictional claims in published maps and institutional affiliations.



Copyright: © 2021 by the authors. Licensee MDPI, Basel, Switzerland. This article is an open access article distributed under the terms and conditions of the Creative Commons Attribution (CC BY) license (<https://creativecommons.org/licenses/by/4.0/>).

Keywords: biomimetic nanochannels; current; fluorescence; dual-signal sensing; H₂S

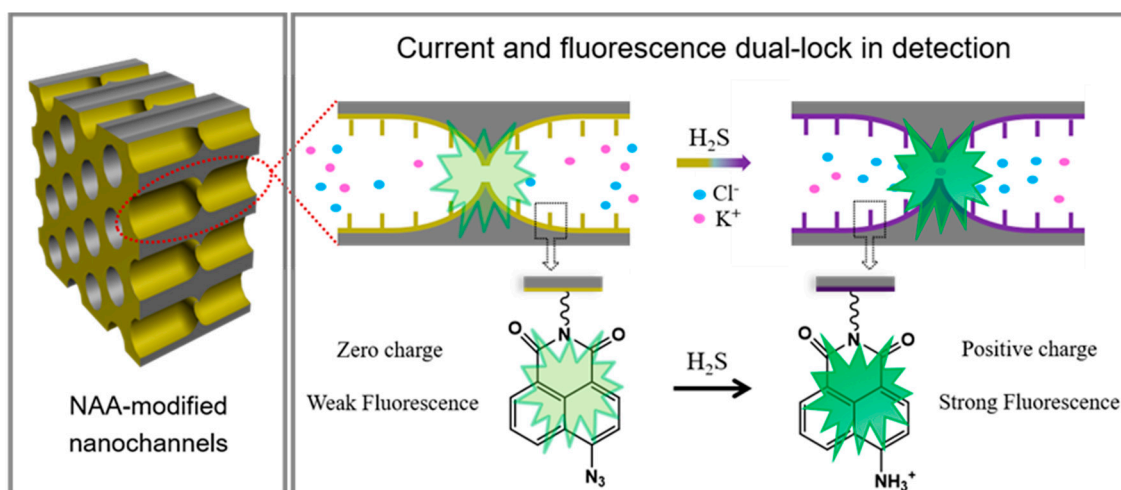
1. Introduction

Ion channels in a biomembrane depend on electrical signal transduction to adjust and change cell behavior in response to external stimuli [1,2]. Inspired by biological channels, artificial nanochannel sensors were developed by monitoring transmembrane ionic current [3–13]. Extensive research efforts have been directed towards the promotion of detection sensitivity for certain targets by laborious regulation of the orifice for the tip region [14–17]. For example, Xia et al. utilized the small aperture in the barrier layer of a nanochannel-ion channel hybrid to achieve ultrasensitive detection of thrombin protein [14]. Furthermore, Xu and coworkers embedded ultra-small nanopipette into living cells, showing the capability for electrochemical monitoring of redox metabolism [17]. Although these existing nanochannels have achieved high recognition ability for specific targets, most sensors only consider individual temporal features from current signals. During the detection process, these electrical signals are vulnerable to be disturbed by channel blockage and damage, leading to false-positive signals and influencing detection accuracy [18,19]. In comparison, if a fluorescence response can be synchronously implemented along with the current signal, the detection confidence levels would be highly improved, as it achieves complementarity, among other spatial-temporal features. Therefore, constructing nanochannels with synchronized fluorescence and current responses is a valuable strategy to increase specific target detection accuracy. Importantly, how to design both these paralleled signal responses within the nanochannels also makes target recognition challenging.

Hydrogen sulfide (H₂S), a biphasic biological mediator in mammals, can drive several types of biological responses—mainly regulatory, stimulatory, and cell-protective—when it is under a physiological concentration [20–27]. Since endogenous H₂S functions as an active modulator, it is easy to be cleared once it is bound to the active sites [28]. Thus,

considering its physiological functions and lability properties *in vivo*, it is necessary to construct a sensitive H₂S sensor to better understand its biological mechanisms. However, the physiological functions in mammals are complicated; they are not only regulated by endogenous H₂S [29]. Therefore, designing artificial analytical tools specific to H₂S is an alternative mode, typically such as colorimetry, chromatography, and metal sulfide precipitation [30–32]. Although H₂S concentrations in plasma and homogenate tissue have been successfully measured, these methods require cumbersome sample pretreatment, and the specificity and sensitivity to H₂S are poor [30–33]. Differently, another fluorescence detection method not only achieves high sensitivity and specificity, but also has the advantages of spatial visualization and *in-situ* H₂S monitoring in living cells [34,35]. However, unfortunately, most of the fluorescent probes are limited in terms of poor water solubility and susceptibility to temperature and pH interference [36]. In recent years, the biomimetic nanochannel sensor has aroused increasing attention from researchers due to its unique confinement effect and capacity to be integrated into electrochemical devices [37–40]. For example, taking advantage of the formation of CuS precipitation in the presence of bovine serum albumin as a biological mineralizer, Song et al. successfully developed an ionic gate in TiO₂ nanochannel for H₂S sensing [39]. Sun et al. applied the BSA aggregation within the channel induced by specific azide reduction by H₂S, to construct an H₂S analysis system [38]. Based on transmembrane current signal change caused by the decrease in effective pore size of nanochannels, these nano detectors are all capable of reaching the detection limit of nM for H₂S. However, the indirect detection mode went through complicated and prolonged activities, which may affect the validity of the current signal.

Herein, we propose a dual-lock nanochannel sensor targeting H₂S with high accuracy by simple reduction of azide groups. The device fuses the spatial stream (fluorescence) and temporal stream (ionic current) in a unified nanochannel platform evoked by specific stimulation. Scheme 1 presents the direct designing experiments paradigm for H₂S identification to expose its spatial–temporal response activities. In this work, the responsive fluorescent probes naphthalic anhydride azide (NAA) were covalently immobilized onto hourglass-shaped nanochannel arrays with tip junctions. Taking advantage of the specific reduction of azido groups by H₂S to amine groups, NAA can be readily reduced to naphthalic anhydride amine. In this case, the inner surface charge of the nanochannel is changed from neutral to positive and fluorophores in probes modified on nanochannels are activated to emit green fluorescence. As a result, these transmembrane ionic current and fluorescence variations output as the temporal and spatial information collaboratively elaborate the response process within the nano spaces. This photoelectric signal synergy can effectively prevent false negative and positive results, and significantly increase the accuracy and reliability of the detection of the nanochannel sensor. Besides, benefiting from the confined effect of tip junction, the nanochannel system can show nM-scale detection sensitivity. Accordingly, these simple tactical decisions of photoelectric dual-insurance monitoring can inspire more start-up nanosensor development.



Scheme 1. Schematic of current and fluorescence dual-lock in the detection of H_2S based on naphthalic anhydride azide (NAA)-modified hourglass-shaped alumina nanochannels. Upon the explosion of H_2S , the azido groups would be reduced into the amino groups, which could trigger surface charges' transformation from neutral to positive charges and fluorescence enhancement from weak to strong.

2. Materials and Methods

2.1. Preparation of Hourglass-Shaped Alumina Nanochannels

100- μm -thick hourglass-shaped alumina nanochannel membrane was successfully built by two-step anodizing combined with an in-situ pore-opening procedure [41,42]. Firstly, a 100 μm -thick aluminum sheet (99.999% purity) was sequentially cleaned by ultrasound in acetone, absolute ethanol, and MilliQ water (18.2 M Ω) for 15 min. Then, electrochemical polishing is performed in a mixed solution of perchloric acid and ethanol (1:4 in volume ratio) at 5 $^\circ\text{C}$ under voltage of 17 V for 3 min. Next, the first anodizing reaction is carried out in a 0.3 M oxalic acid solution at 5 $^\circ\text{C}$ under anodizing voltage of 50 V. This oxidation takes about an hour on each side. Thereinto, Al foil serves as the anode, while the graphite plate serves as the cathode. In this way, a porous aluminum oxide layer with less thickness is grown on both sides of the aluminum sheet, but it was out of order. Thus, the resulted sample membrane needed to be immersed in a mixture of 6 wt% phosphoric acid and 3.5 wt% chromium trioxide at 90 $^\circ\text{C}$ to remove the oxidation layer, and each side was etched for an hour. As a result, the hemispherical concaves are left on both sides of the aluminum surface, which will be conducive to the orderly growth of porous layers during the second oxidation. The conditions of the second anodization are the same as those of the first. In this process, the Al_2O_3 nanoarrays on both sides grow simultaneously until two-side barrier layers counter at the middle position. At this point, the anodizing current goes to zero, which indicated that the entire aluminum substrate is oxidized to alumina. Finally, the resulted porous alumina membrane was still immersed in the oxalic acid electrolyte for 30 min to ream in situ. The middle barrier layer was punched through to form the small tip junction, while the two sides of the nanoarrays have large pore ends. Thus, a porous hourglass-shaped alumina nanochannel membrane was successfully built. The resulted nanochannels exhibited symmetrical geometry with a small tip junction and large pore ends at the two sides. Its detail morphology was characterized by scanning electron microscopy (SEM).

2.2. Synthesis of the Probe Naphthalic Anhydride-Azide

The probe of the naphthalic anhydride-azide conjugate was facily synthesized using a two-step substitution reaction route according to the reported method [43,44]. The structure of the title compound was verified by hydrogen-nuclear magnetic resonance (^1H NMR), mass spectrum (MS), and infrared spectrum (IR spectra).

2.3. Construction of Functionalized Nanochannels

Firstly, nanochannels were aminated with (3-Aminopropyl) triethoxysilane (APTES). The alumina membrane was boiled with hydrogen peroxide for an hour to activate the hydroxyl groups on the surface of the channel. Taking advantage of the coupling properties of amino silane for inorganic materials and organic components, the membrane was immersed in 16% APTES for an hour to aminate the inner wall of the channels.

Secondly, carboxyl groups of probes were activated by a conjugate with N-hydroxysuccinimide (NHS) to yield NHS-protected intermediate. During this process, a certain amount of naphthalic anhydride-azide probes were first dissolved in a mixture of DMSO and absolute alcohol at 1:9 in volume ratio. Then the given 1-Ethyl-3-(3-dimethylaminopropyl) carbodiimide (EDC) and NHS were added into the mixed solution and stirred for an hour to produce amine-reactive ester molecules.

Thirdly, probes were immobilized onto APTES-modified nanochannel surface through covalent bonds. Having achieved the above two steps of pretreatment, the APTES-modified nanochannel membrane (step 1) was soaked into a solution containing amine-reactive ester probes (step 2) over a designed period. As a result, the intermediates were covalently condensed onto the pore surface through the formation of a stable amide linkage. Finally, the entire membrane was ultrasonically cleaned three times in an ethanol solution to remove the free probes and other impurities by physical adsorption.

2.4. Response of Functionalized Nanochannels to H_2S

The response of the nanochannel system to the analytes is carried out by immersing the functionalized membrane directly into the analyte solution at a specific concentration for a designed period. The chemical reaction of the nanochannel sensorial platform is a specific reduction of the 4-position azide group ($-N_3$) on 1,8-naphthalic anhydride to an amino group ($-NH_2$) by H_2S . The simplified equation is shown as: $-N_3 + H_2S = -NH_2$, achieving the successful transformation from azide groups to amino groups.

2.5. Analysis and Characterization

2.5.1. Ionic Current Measurement

The electric signal was characterized by monitoring the ionic current across the nanochannel membrane. It, in the form of a current-voltage (I - V) curve, is recorded in a Keithley 6487 picoammeter (Keithley Instruments, Cleveland, OH, USA). A functionalized nanochannel was fixed between two half-cells with 1 mM potassium chloride (KCl) aqueous as electrolyte solutions in each electrochemical reservoir. Moreover, two Ag/AgCl electrodes connected with a Keithley 6487 picoammeter were settled in half-cells, respectively. Then the picoammeter as a source of voltage will apply a transmembrane potential to induce the ionic transportation, and the voltage was stepped between +2 V to −2 V with 100 mV steps and 0.5 s time delay.

2.5.2. Fluorescence Properties Measurement

Fluorescence spectra and fluorescence imaging were collected on HORIBA FluoroLog-3 Modular Spectrofluorometer (Horiba Instruments, Acal BFi Nederland) and Carl Zeiss LSM710 confocal microscope (Carl Zeiss Pty Ltd., Sydney, Australia), respectively.

2.5.3. Characterization

The surface and cross-section morphologies of the hourglass-shaped alumina nanochannels were observed by environmental scanning electron microscope (SEM, FEI Quanta FEG 250). 1H NMR, MS, and IR spectra were adopted to determine the probes' structure. UV-Vis absorption spectra were performed using a Shimadzu UV-1800 UV/Visible scanning spectrophotometer (Shimadzu, Kyoto, Japan). During the entire modification and response process, X-ray photoelectron spectroscopy (XPS) and contact angle (CA) measurement were employed to analyze the elementary composition and water wettability on the nanochannel

surface by an ESCALAB 250Xi XPS (Thermo Fisher Scientific, Waltham, MA, USA) and an OCA40 contact-angle system (DataPhysics, Filderstadt, Germany), respectively.

3. Results and Discussions

3.1. Construction and Modification of the Artificial Nanochannels

The hourglass-shaped Al_2O_3 nanochannels were successfully built by two-sided anodic oxidation combined with in-situ pore-opening treatment [41]. This channel shows a symmetrical geometry as a whole with an opening pore at both ends and a small pore at the center. As investigated by scanning electron microscopy (SEM) in Figure S1, the thickness of the alumina membrane is about $100\ \mu\text{m}$. And at its center, there is a thin dividing line (Figure S1a,b). From the corresponding magnified image, a tiny tip junction that joins two ends of the nanochannel was observed. Comparing with the tip, the pore diameters at both top and bottom sides of as-prepared hourglass-shaped alumina nanochannels were estimated to be about $30\ \text{nm}$ (Figure S1c,d). Therefore, this tip junction plays a critical role in the confining behavior of nanochannels.

Anodized channels on aluminum substrates possess abundant hydroxyl groups. Considering that our goal was to covalently immobilize the recognition probes on the channel wall, the Al_2O_3 membrane was firstly treated with (3-Aminopropyl) triethoxysilane (APTES) to produce an amine surface, aiming to covalently immobilize the recognition probes on the channel wall (Figure 1a) [42]. During the covalent immobilization, these terminal groups will further react with the carboxylic group in fluorescent probes. As shown in Figure 1b, the pure Al_2O_3 membrane exhibited strong hydrophilicity at a CA of 43.4° . APTES crosslinks sharply reduced the water wettability of the membrane, showing that the CA increased to 84.2° . Such change will temporarily inhibit ion transport behavior across the membrane to a certain extent, which is directly manifested on an ionic current reduction shown in the current voltage (I - V) curve (Figure 1c). We can see from this XPS spectrum of silicon element in inset that, as expected, compared to the alumina membrane, a new Si2p peak at about $101.7\ \text{eV}$ belonging to APTES appeared after achieving APTES modification [42]. In order to further intuitively prove the successful grafting of APTES, FITC was used as a fluorescent marker to react with the terminal amino groups, which caused the membrane to turn yellow and emitted green fluorescence by laser-scanning confocal microscope (LSCM) imaging (Figure 1d) [42].

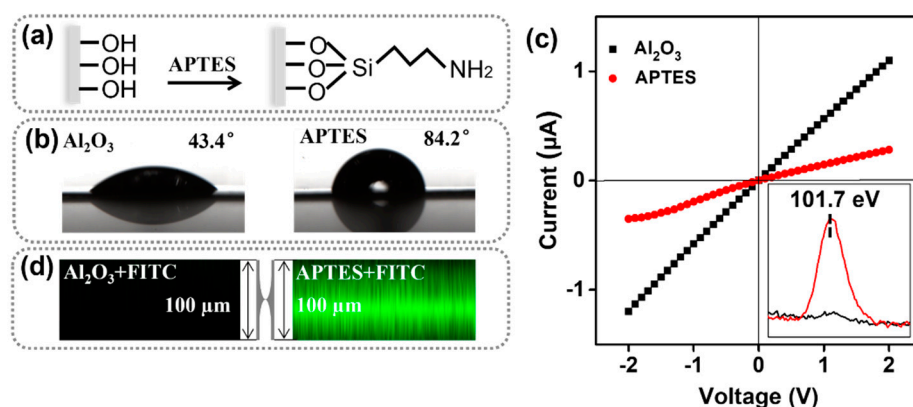


Figure 1. (a) Schematic diagram of the modification of alumina nanochannels with APTES. The characteristic for successful modification of APTES by (b) CA measurement, (c) I - V curve (the inset is XPS spectrum in the Si2p core level region), and (d) laser scanning confocal microscope (LSCM) imaging. The diagram in the middle shows the cross-section of a typical single channel in the alumina membrane.

Meanwhile, we elaborately designed a multifunctional naphthalic anhydride-azide (NAA) fluorescent probe by a simple two-step substitution reaction (Figure S2) [43,44]. The ^1H NMR spectrum (Figure S3), MS (Figure S4), and IR spectrum (Figure S5) prove

the successful substitution of a carboxyl group and azido group on the opposite side of naphthalic anhydride. The resulted NAA probe is fused with a fluorophore chromophore (naphthalic anhydride) carrying two available groups (carboxyl and azido groups) on either side. Thereinto, an azido group at the 4-position of naphthalic anhydride acts as a recognition element that specifically responds to H₂S. Because the azide group can be effectively reduced to an amino group by H₂S, the intramolecular charge transfer (ICT) was restored and thus a green fluorescence is produced [45]. As shown in Figure S6a, a visualized color change of probe solution from light green to yellow can be observed in the absence and presence of H₂S. Upon exposure to UV radiation, the strong green fluorescence was readily apparent after the addition of aqueous NaHS as the H₂S source (Figure S6b). In addition, UV-Vis absorption spectra (Figure S6c) and fluorescence spectra (Figure S6d) of the probe solution further showed a good response capacity. The intensity of absorption and fluorescence increased markedly with than without H₂S.

In addition to the azide group as a recognition site, this probe also carries another functional carboxyl group on the opposite side. It, as a covalent anchoring site, was able to steadily attach onto the amine channel surface through amido linkage with the activation of EDC/NHS (Figure S7a) [42,46]. Moreover, the ionic transduction is also sensitive to the modification state due to the confinement effect of the tip junction. Thus, these factors such as coupling agent concentration, probe concentration, and modification time were also explored to reach the most appropriate modification state. As shown in Figure S7b–d, the content of the coupling agent has little effect on the ion transport behavior, but both the probe concentration and modification time have strong impacts on ionic transport and response performance. This is because a light probe concentration or a short period of time will make the surface modification insufficient, while an excessively high probe concentration or long time will cause the blocking of the tip interface and deterioration of ion transport performance in the end. So, comparing the current responsive result with different probe concentrations and modification time, here, we choose the 5 mM and 10 h as the optimum probe concentration and modification time, respectively. Once this modification completes, all the silanized nanochannels develop to light yellow (Figure S8), which is close to the color of the probes' bulk solution. Importantly, the terminal azide site will be exposed inside the nanochannel without the obstructing execution of its response to H₂S.

3.2. The Dual Lock-in Detection Mechanism

The dual-responsive actuation sensing mechanism for synchronized spatial-temporal monitoring is mainly studied by the variation of the signal in both ionic current and fluorescence intensity upon H₂S stimulus. That, as a practical example, can verify the availability of dual-signal-output in a unified nanochannel functionalized by designed fluorescent probes. As shown in Figure 2a, the ionic current of NAA-modified nanochannels is gradually increased with the addition of NaHS. This is attributed to the incremental surface positive charges and water wettability. Upon H₂S response, the terminal azido group from the probe is converted to an amino group, which is positively charged under neutral pH conditions (pH ≈ 7). Then these rich protonated amino groups (-NH₃⁺) appeared on the inner surface of nanochannels improve the hydrophilicity of the nanochannel membrane (Figure 2b). Meanwhile, due to the electrostatic actions within nanoscale spaces, the formation of positive surface charges will cause more chloride ions to be attracted into the channels (Figure 2c). As a result, the transmembrane ionic current rises gradually when exposed to H₂S at increasing concentrations. This indicated a gradual change in surface chemical composition within channels from anhydride azide to anhydride amine. The pH-dependent measurements of functionalized nanochannels before and after NaHS response also demonstrated the successful conversion of the azide to amino groups (Figure S9).

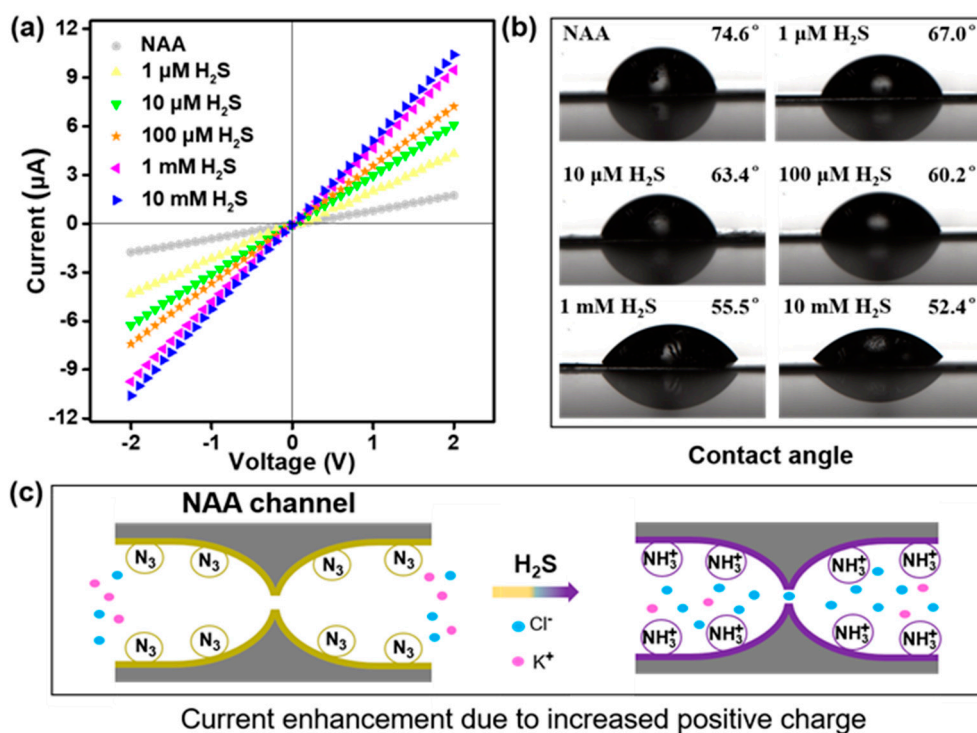


Figure 2. Electrical signal response on H₂S of functionalized NAA-modified nanochannels. (a) *I-V* curves of the nanochannel membrane upon incremental H₂S concentration in 1 mM KCl. (b) The evolution for wettability of the nanochannel membrane upon incremental H₂S concentration via CA measurement. (c) The schematic diagram of the mechanism of transmembrane current increase upon H₂S exposure.

Not only that, the chemical response of probes onto channels to H₂S presents regular changes in optical properties as well. As shown in Figure 3a, the redshift of the absorption band and the increase in absorption intensity at about 430 nm with the addition of NaHS can be observed. This means it allows for enhanced green–yellow-light harvesting. Therefore, by applying an excitation light source at 450 nm, the probe-modified Al₂O₃ nanochannels will demonstrate a fluorescent-enhanced phenomenon at the wavelength of 521 nm upon the stimulus of incremental H₂S (Figure 3b). The fluorescence (*F*) at 521 nm showed a good linear relationship with the logarithm (Log*C*) of H₂S concentration (Figure S10), which can be employed as the optical quantitative signal. Besides, the fluorescence information visualization can be imaged by LSCM images. Once this functionalized nanochannel was exposed to H₂S, a strong green fluorescence could be clearly observed. And with the addition of NaHS, the fluorescence intensity was enhanced apparently (Figure 3c). In a word, this novel nanosensor also has an efficient optical signal output for H₂S responsiveness. This, similarly, is because of the reduction of azide groups by H₂S to amino. As shown in Figure 3d, the azido group at the 4-position of NAA probe blocked the ICT process and caused the nanochannels to be fluorescence quenched. But with the employment of H₂S stimulus, the azido group would be converted to an amino group. In this case, the ICT from amine to naphthalic anhydride could be recovered and fluorescence is produced. Accordingly, the synchronized switch in current and fluorescence dual signals can be facily achieved by immobilizing designed fluorescent probe molecules into hourglass-shaped Al₂O₃ nanochannels. This essentially developed a parallel temporal-spatial detection mechanism. Additionally, the detailed deconvoluted N1s XPS spectra also demonstrated that H₂S interacted with the azide group of NAA probes on the Al₂O₃ membrane successfully (Figure 3e). In NAA channel, the N1s spectra can be fitted into a large peak at around 399.2 eV (pink dotted line) and a small peak at about 400.9 eV (green dotted line). More specifically, the large peak corresponds to nitrogen elements on both sides of azide, while the small peak was assigned to nitrogen element in the middle of azide as well as C-N.

After treating with NaHS solution (100 μM), the above two peaks are transformed into a single peak at about 399.8 eV, all belonging to C-N. The disappearance of the azide peak clearly shows that the azide group is reduced to an amino group by H_2S . Although this nanochannel is endowed with a sensing function for H_2S , no changes in its structural morphology during modification and response process were observed (Figure S11). The all-round results proved the response behavior is attributed to the chemical reaction of the surface probe rather than the change in channel structure. Accordingly, with a new combining method of photochemistry and electrochemistry, a solid-state nanochannel sensor for H_2S was successfully set up. The combination of current and fluorescence allows for more precise and accurate quantitative monitoring of the targets.

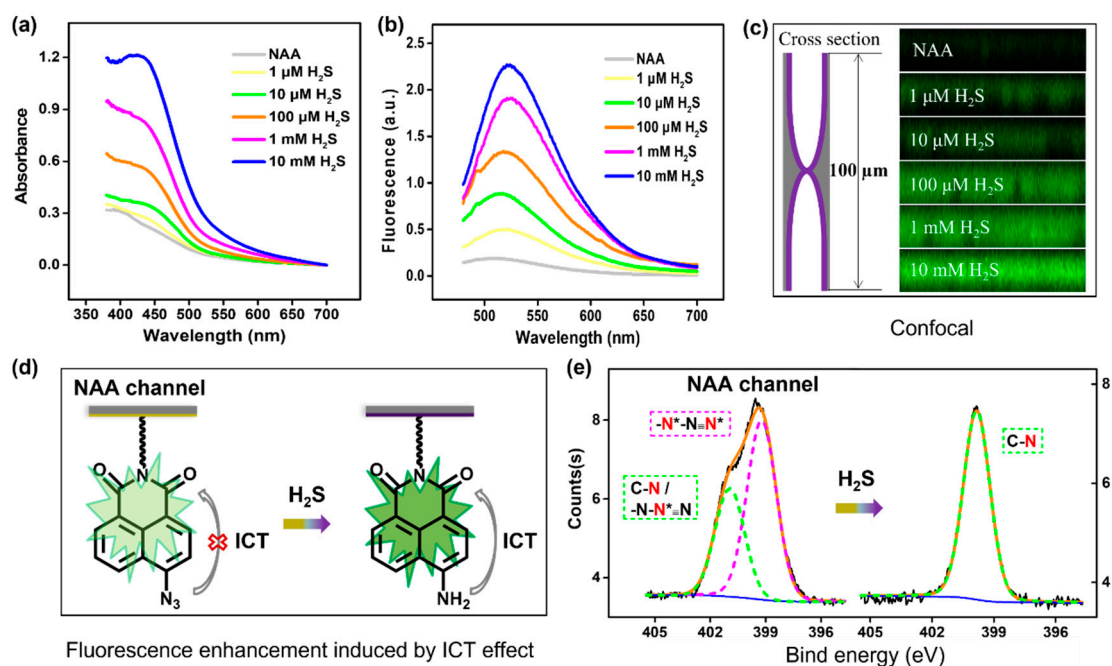


Figure 3. Optical responses of functionalized NAA-modified nanochannels towards H_2S . (a) absorption spectra, (b) fluorescence spectra, and (c) LSCM images of the nanochannels upon incremental H_2S concentration. The diagram on the left represents the cross-section of a typical single channel with 100 μm thickness. (d) ICT mechanism of NAA probe based on azide reduction by H_2S . Green fluorescence was recovered upon H_2S exposure. (e) The XPS spectra of nitrogen element of NAA nanochannel membrane before and after H_2S treatment.

3.3. Selectivity, Reaction Time, and Sensitivity of the Nanosensor

The selectivity, reaction rate, and sensitivity of the sensor are three important criteria for sample analysis. To confirm the specific selectivity of the sensor towards H_2S , the NAA-modified nanochannels were exposed to diversified targets component at 100 μM concentration (anions such as SO_4^{2-} , $\text{S}_2\text{O}_3^{2-}$, CO_3^{2-} , NO_3^- , NO_2^- , Cl^- , Br^- , and OH^- , reactive oxygen species such as HClO and H_2O_2 , as well as glucose). Obviously, comparing to other analytes, the variation of the ionic current at -2 V only treated by H_2S is the largest ≈ 5.7 μA (from -1.76 μA to -7.46 μA), as indicated in the I - V curves of Figure 4a. In Figure 4b, the ionic current at -2 V is continuing to increase over a period of 120 min. However, after 120 min, no increase in current was observed, which suggests that the redox reaction caused by H_2S and probes has reached a saturation point. Moreover, the sensitivity was measured by adjusting the concentrations of H_2S . As shown in Figure 4c, with the continuous adding of H_2S ranging from 1 μM to 10 mM, the ionic current kept on increasing. By plotting the change in the ionic current response (ΔI) against the logarithm of H_2S concentration ($\text{Log } C$), a linear relationship is obtained in a wide range of concentrations (from 1 μM to 1 mM). Its typical calibration curve is $\Delta I = -1.79 \text{ Log } C - 2.42$ with a correlation coefficient of 0.98. Thereinto, ΔI (μA) is defined as the change of the ionic

current at -2.0 V relative to the background current ($\text{cH}_2\text{S} = 0.0 \mu\text{M}$). As reported, the lowest detection limit (LOD) of the nanochannel sensor could be calculated by the formula, $\text{LOD} = 3 \text{SD}/\text{N}$, where SD is the standard deviation of the blank, N is the slope of the calibration curve [9,47]. In our study, the value of SD and N are 0.0218 and 1.79, respectively. Therefore, the LOD of the nanochannel sensor to H_2S is estimated as 36.6 nM. The linear relationship makes the nanochannel sensor promising for the quantitative determination of H_2S concentration in the nanomolar to micromole range. In addition, a linear relationship can be established using the slope of I - V curves and the logarithm of concentration. The LOD calculated from this line is also 36.6 nM (Figure S12).

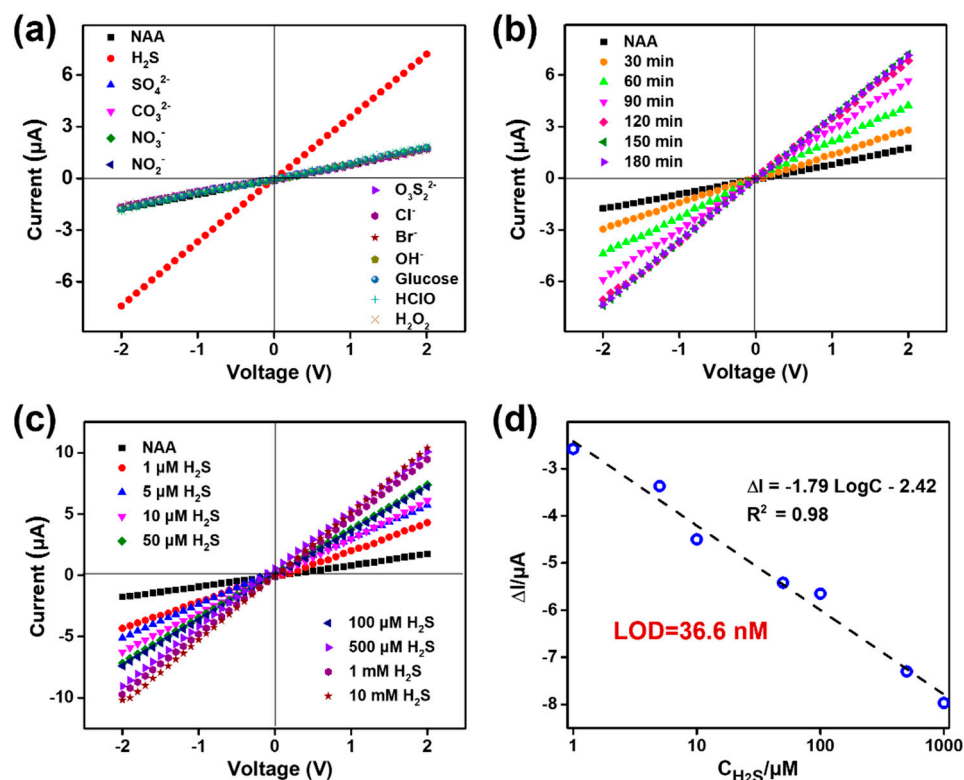


Figure 4. Response performance of NAA-modified nanochannels towards H_2S including selectivity from various anion or oxidizers, reaction equilibrium time, and sensitivity using I - V characteristic. (a) I - V curves response of NAA-modified nanochannels upon the treatment of different-type targets (H_2S , SO_4^{2-} , CO_3^{2-} , NO_3^{2-} , NO_2^{2-} , $\text{S}_2\text{O}_3^{2-}$, Cl^- , Br^- , OH^- , glucose, HClO , and H_2O_2 .) at $100 \mu\text{M}$ concentration. Selectivity of the nanosensor towards H_2S over other components. (b) I - V curves of NAA-modified nanochannels upon treatment of $100 \mu\text{M}$ H_2S for incremental time. The ionic current increased as reaction time prolonged and the response system attained equilibrium status at about 120 min. (c) I - V curves response of NAA-modified nanochannels upon the treatment of incremental levels of H_2S from $1 \mu\text{M}$ to 10 mM for 120 min and (d) a linear relationship between the difference of transmembrane ionic current before and after H_2S treatment and the logarithm of concentration of H_2S . The lowest detection limit has been calculated as 36.6 nM.

4. Conclusions

In conclusion, we proposed a current and fluorescence dual lock-in detection mode, by immobilizing fluorescent probe molecules onto biomimetic nanochannels. This platform has the advantage of providing parallel spatial-temporal information to represent the responsive process within nanochannels and thus results in an increase in detection credibility. Combining fluorescence with current measurement functions, the sensor can reliably eliminate false positives results. This study uses NAA-modified nanochannels for H_2S monitoring as an example to demonstrate the synchronous change of photoelectric signals. Upon H_2S stimulus, the azido groups of probes on the channel surface are reduced

to amino groups, which can lead to an increase in both surface charge and fluorescence intensity. This nanosystem exhibited good selectivity for H₂S and sensitivity at nanomole. We believe that the fluorescent probe-functionalized nanochannel sensor will provide a promising approach for capturing synchronized photoelectric signals and parallel spatiotemporal monitoring. The photoelectric sensors are expected to be used for reliable and sensitive detection of various analytes.

Supplementary Materials: The following are available online at <https://www.mdpi.com/article/10.3390/chemosensors9110298/s1>, Figure S1: SEM images of the hourglass-shaped alumina nanochannel, Figure S2: the synthesis of naphthalic anhydride-azide probe, Figure S3: the ¹H NMR spectrum of mediate compound and naphthalic anhydride-azide probe, Figure S4: the MS of naphthalic anhydride-azide probe, Figure S5: the IR spectrum of naphthalic anhydride-azide probe, Figure S6: the photographic images of probe solution, UV-Vis absorption spectra and fluorescence spectra of probe solution before and after H₂S stimulus, Figure S7: *I-V* curves of NAA channel upon different EDC/NHS concentration, different probe solution, and different modification time, Figure S8: optical photograph nanochannels before and after modification of probe molecules, Figure S9: The pH-dependent *I-V* curve measurements of functionalized nanochannels before and after treatment with NaHS, Figure S10: The quantitative linear relationship between the fluorescence with the H₂S concentration, Figure S11: SEM images of alumina nanochannels after treatment with APTES, probe and NaHS, Figure S12: The linear relationship between the slope of *I-V* curves with the H₂S concentration.

Author Contributions: Conceptualization, I.W., D.Z. and X.Z.; methodology, D.Z. and X.Z.; software, D.Z.; validation, I.W., D.Z. and X.Z.; formal analysis, I.W.; investigation, I.W. and D.Z.; resources, X.Z.; data curation, I.W. and D.Z.; writing—original draft preparation, I.W. and D.Z.; writing—review and editing, D.Z. and X.Z.; visualization, D.Z.; supervision, X.Z.; project administration, X.Z.; funding acquisition, X.Z. All authors have read and agreed to the published version of the manuscript.

Funding: This research was funded by the Science and Technology Development Fund, Macau SAR grant number 0114/2019/A2, 019/2017/AMJ and 0085/2020/A2; the Research Grant of University of Macau, grant number MYRG2019-00051-FHS and MYRG2017-00066-FHS. We also thank the core facilities at the Faculty of Health Sciences, especially the drug development core, bioimaging, and stem cell core for their excellent services.

Institutional Review Board Statement: Not applicable.

Informed Consent Statement: Not applicable.

Data Availability Statement: Not applicable.

Conflicts of Interest: The authors declare no conflict of interest.

References

1. Prindle, A.; Liu, J.; Asally, M.; Ly, S.; Garcia-Ojalvo, J.; Suel, G.M. Ion channels enable electrical communication in bacterial communities. *Nature* **2015**, *527*, 59–63. [CrossRef]
2. Doyle, D.A.; Morais Cabral, J.; Pfuetzner, R.A.; Kuo, A.; Gulbis, J.M.; Cohen, S.L.; Chait, B.T.; MacKinnon, R. The structure of the potassium channel: Molecular basis of K⁺ conduction and selectivity. *Science* **1998**, *280*, 69–77. [CrossRef]
3. Wu, Y.; Yang, G.; Lin, M.; Kong, X.; Mi, L.; Liu, S.; Chen, G.; Tian, Y.; Jiang, L. Continuously Tunable Ion Rectification and Conductance in Submicrochannels Stemming from Thermoresponsive Polymer Self-Assembly. *Angew. Chem. Int. Ed. Engl.* **2019**, *58*, 12481–12485. [CrossRef]
4. Xie, G.; Xiao, K.; Zhang, Z.; Kong, X.Y.; Liu, Q.; Li, P.; Wen, L.; Jiang, L. A Bioinspired Switchable and Tunable Carbonate-Activated Nanofluidic Diode Based on a Single Nanochannel. *Angew. Chem. Int. Ed. Engl.* **2015**, *54*, 13664–13668. [CrossRef]
5. Liu, Q.; Xiao, K.; Wen, L.; Lu, H.; Liu, Y.; Kong, X.Y.; Xie, G.; Zhang, Z.; Bo, Z.; Jiang, L. Engineered Ionic Gates for Ion Conduction Based on Sodium and Potassium Activated Nanochannels. *J. Am. Chem. Soc.* **2015**, *137*, 11976–11983. [CrossRef]
6. Zhao, X.P.; Wang, S.S.; Younis, M.R.; Xia, X.H.; Wang, C. Asymmetric Nanochannel-Ionchannel Hybrid for Ultrasensitive and Label-Free Detection of Copper Ions in Blood. *Anal. Chem.* **2018**, *90*, 896–902. [CrossRef]
7. Shang, X.; Xie, G.; Kong, X.Y.; Zhang, Z.; Zhang, Y.; Tian, W.; Wen, L.; Jiang, L. An Artificial CO₂-Driven Ionic Gate Inspired by Olfactory Sensory Neurons in Mosquitoes. *Adv. Mater.* **2017**, *29*, 1603884. [CrossRef]
8. Wu, K.; Kong, X.Y.; Xiao, K.; Wei, Y.; Zhu, C.; Zhou, R.; Si, M.; Wang, J.; Zhang, Y.; Wen, L. Engineered Smart Gating Nanochannels for High Performance in Formaldehyde Detection and Removal. *Adv. Funct. Mater.* **2019**, *29*, 1807953. [CrossRef]
9. Zhao, X.-P.; Cao, J.; Nie, X.-G.; Wang, S.-S.; Wang, C.; Xia, X.-H. Label-free monitoring of the thrombin–aptamer recognition reaction using an array of nanochannels coupled with electrochemical detection. *Electrochem. Commun.* **2017**, *81*, 5–9. [CrossRef]

10. Burns, J.R.; Seifert, A.; Fertig, N.; Howorka, S. A biomimetic DNA-based channel for the ligand-controlled transport of charged molecular cargo across a biological membrane. *Nat. Nanotechnol.* **2016**, *11*, 152–156. [[CrossRef](#)] [[PubMed](#)]
11. Liu, N.; Jiang, Y.; Zhou, Y.; Xia, F.; Guo, W.; Jiang, L. Two-way nanopore sensing of sequence-specific oligonucleotides and small-molecule targets in complex matrices using integrated DNA supersandwich structures. *Angew. Chem. Int. Ed. Engl.* **2013**, *52*, 2007–2011. [[CrossRef](#)]
12. Cao, J.; Zhao, X.P.; Younis, M.R.; Li, Z.Q.; Xia, X.H.; Wang, C. Ultrasensitive Capture, Detection, and Release of Circulating Tumor Cells Using a Nanochannel-Ion Channel Hybrid Coupled with Electrochemical Detection Technique. *Anal. Chem.* **2017**, *89*, 10957–10964. [[CrossRef](#)]
13. Freedman, K.J.; Otto, L.M.; Ivanov, A.P.; Barik, A.; Oh, S.H.; Edell, J.B. Nanopore sensing at ultra-low concentrations using single-molecule dielectrophoretic trapping. *Nat. Commun.* **2016**, *7*, 10217. [[CrossRef](#)] [[PubMed](#)]
14. Zhao, X.P.; Zhou, Y.; Zhang, Q.W.; Yang, D.R.; Wang, C.; Xia, X.H. Nanochannel-Ion Channel Hybrid Device for Ultrasensitive Monitoring of Biomolecular Recognition Events. *Anal. Chem.* **2019**, *91*, 1185–1193. [[CrossRef](#)] [[PubMed](#)]
15. Xu, X.; Li, C.; Zhou, Y.; Jin, Y. Controllable Shrinking of Glass Capillary Nanopores Down to sub-10 nm by Wet-Chemical Silanization for Signal-Enhanced DNA Translocation. *ACS Sens.* **2017**, *2*, 1452–1457. [[CrossRef](#)] [[PubMed](#)]
16. Jiao, S.; Liu, L.; Wang, J.; Ma, K.; Lv, J. A Novel Biosensor Based on Molybdenum Disulfide (MoS₂) Modified Porous Anodic Aluminum Oxide Nanochannels for Ultrasensitive microRNA-155 Detection. *Small* **2020**, *16*, e2001223. [[CrossRef](#)] [[PubMed](#)]
17. Song, J.; Xu, C.H.; Huang, S.Z.; Lei, W.; Ruan, Y.F.; Lu, H.J.; Zhao, W.; Xu, J.J.; Chen, H.Y. Ultrasmall Nanopipette: Toward Continuous Monitoring of Redox Metabolism at Subcellular Level. *Angew. Chem. Int. Ed. Engl.* **2018**, *57*, 13226–13230. [[CrossRef](#)] [[PubMed](#)]
18. Liu, J.; Fu, B.; Zhang, Z. Ionic Current Rectification Triggered Photoelectrochemical Chiral Sensing Platform for Recognition of Amino Acid Enantiomers on Self-Standing Nanochannel Arrays. *Anal. Chem.* **2020**, *92*, 8670–8674. [[CrossRef](#)] [[PubMed](#)]
19. Xu, X.; Zhao, W.; Gao, P.; Li, H.; Feng, G.; Zhao, Z.; Lou, X. Coordination of the electrical and optical signals revealing nanochannels with an ‘onion-like’ gating mechanism and its sensing application. *NPG Asia Mater.* **2016**, *8*, e234. [[CrossRef](#)]
20. Donnarumma, E.; Trivedi, R.K.; Lefer, D.J. Protective Actions of H₂S in Acute Myocardial Infarction and Heart Failure. *Compr. Physiol.* **2017**, *7*, 583–602.
21. King, A.L.; Lefer, D.J. Cytoprotective actions of hydrogen sulfide in ischaemia-reperfusion injury. *Exp. Physiol.* **2011**, *96*, 840–846. [[CrossRef](#)] [[PubMed](#)]
22. Polhemus, D.J.; Lefer, D.J. Emergence of hydrogen sulfide as an endogenous gaseous signaling molecule in cardiovascular disease. *Circ. Res.* **2014**, *114*, 730–737. [[CrossRef](#)] [[PubMed](#)]
23. Reiffenstein, R.J.; Hulbert, W.C.; Roth, S.H. Toxicology of hydrogen sulfide. *Annu Rev. Pharmacol. Toxicol.* **1992**, *32*, 109–134. [[CrossRef](#)] [[PubMed](#)]
24. Yang, G.; Wu, L.; Jiang, B.; Yang, W.; Qi, J.; Cao, K.; Meng, Q.; Mustafa, A.K.; Mu, W.; Zhang, S.; et al. H₂S as a physiologic vasorelaxant: Hypertension in mice with deletion of cystathionine gamma-lyase. *Science* **2008**, *322*, 587–590. [[CrossRef](#)]
25. Hu, X.; Luan, L.; Guan, W.; Zhang, S.; Li, B.; Ji, W.; Fan, H. Hydrogen sulfide attenuates isoflurane-induced neuroapoptosis and cognitive impairment in the developing rat brain. *BMC Anesthesiol.* **2017**, *17*, 123. [[CrossRef](#)]
26. Shefa, U.; Kim, M.S.; Jeong, N.Y.; Jung, J. Antioxidant and Cell-Signaling Functions of Hydrogen Sulfide in the Central Nervous System. *Oxid. Med. Cell. Longev.* **2018**, *2018*, 1873962. [[CrossRef](#)]
27. Dallas, M.L.; Al-Owais, M.M.; Hettiarachchi, N.T.; Vandiver, M.S.; Jarosz-Griffiths, H.H.; Scragg, J.L.; Boyle, J.P.; Steele, D.; Peers, C. Hydrogen sulfide regulates hippocampal neuron excitability via S-sulfhydration of Kv2.1. *Sci. Rep.* **2021**, *11*, 8194. [[CrossRef](#)]
28. Wang, Z.J.; Wu, J.; Guo, W.; Zhu, Y.Z. Atherosclerosis and the Hydrogen Sulfide Signaling Pathway—Therapeutic Approaches to Disease Prevention. *Cell. Physiol. Biochem.* **2017**, *42*, 859–875. [[CrossRef](#)]
29. Li, L.; Moore, P.K. An overview of the biological significance of endogenous gases: New roles for old molecules. *Biochem. Soc. Trans.* **2007**, *35*, 1138–1141. [[CrossRef](#)]
30. Cha, J.-H.; Kim, D.-H.; Choi, S.-J.; Koo, W.-T.; Kim, I.-D. Sub-Parts-per-Million Hydrogen Sulfide Colorimetric Sensor: Lead Acetate Anchored Nanofibers toward Halitosis Diagnosis. *Anal. Chem.* **2018**, *90*, 8769–8775. [[CrossRef](#)]
31. Furne, J.; Saeed, A.; Levitt, M.D. Whole tissue hydrogen sulfide concentrations are orders of magnitude lower than presently accepted values. *AJP-Regul. Integr. Comp. Physiol.* **2008**, *295*, R1479–R1485. [[CrossRef](#)] [[PubMed](#)]
32. Ishigami, M.; Hiraki, K.; Umemura, K.; Ogasawara, Y.; Ishii, K.; Kimura, H. A Source of Hydrogen Sulfide and a Mechanism of Its Release in the Brain. *Antioxid. Redox Signal.* **2009**, *11*, 205–214. [[CrossRef](#)] [[PubMed](#)]
33. Jia, Y.; Guo, Y.; Wang, S.; Chen, W.; Zhang, J.; Zheng, W.; Jiang, X. Nanocrystalline cellulose mediated seed-growth for ultra-robust colorimetric detection of hydrogen sulfide. *Nanoscale* **2017**, *9*, 9811–9817. [[CrossRef](#)] [[PubMed](#)]
34. Wang, C.; Cheng, X.; Tan, J.; Ding, Z.; Wang, W.; Yuan, D.; Li, G.; Zhang, H.; Zhang, X. Reductive cleavage of C=C bond as a new strategy for turn-on dual fluorescence in effective sensing of H₂S. *Chem. Sci.* **2018**, *9*, 8369–8374. [[CrossRef](#)] [[PubMed](#)]
35. Henthorn, H.A.; Pluth, M.D. Mechanistic Insights into the H₂S-Mediated Reduction of Aryl Azides Commonly Used in H₂S Detection. *J. Am. Chem. Soc.* **2015**, *137*, 15330–15336. [[CrossRef](#)]
36. Yassine, O.; Shekhah, O.; Assen, A.H.; Belmabkhout, Y.; Salama, K.N.; Eddaoudi, M. H₂S Sensors: Fumarate-Based fcu-MOF Thin Film Grown on a Capacitive Interdigitated Electrode. *Angew. Chem. Int. Ed.* **2016**, *55*, 15879–15883. [[CrossRef](#)]
37. Sun, Z.; Yuan, H.; Liu, Z.; Han, B.; Zhang, X. A Highly Efficient Chemical Sensor Material for H₂S: α-Fe₂O₃ Nanotubes Fabricated Using Carbon Nanotube Templates. *Adv. Mater.* **2005**, *17*, 2993–2997. [[CrossRef](#)]

38. Zhang, R.; Chen, X.; Sun, Z.; Chen, S.; Gao, J.; Sun, Y.; Li, H. Switchable Nanochannel Biosensor for H₂S Detection Based on an Azide Reduction Reaction Controlled BSA Aggregation. *Anal. Chem.* **2019**, *91*, 6149–6154. [[CrossRef](#)]
39. Guo, J.; Yang, L.; Xu, H.; Zhao, C.; Dai, Z.; Gao, Z.; Song, Y. Biomineralization-Driven Ion Gate in TiO₂ Nanochannel Arrays for Cell H₂S Sensing. *Anal. Chem.* **2019**, *91*, 13746–13751. [[CrossRef](#)]
40. Nesakumar, N.; Kesavan, S.; Li, C.-Z.; Alwarappan, S. Microfluidic Electrochemical Devices for Biosensing. *J. Anal. Test.* **2019**, *3*, 3–18. [[CrossRef](#)]
41. Zhang, D.; Zhou, S.; Liu, Y.; Fan, X.; Zhang, M.; Zhai, J.; Jiang, L. Self-Assembled Porphyrin Nanofiber Membrane-Decorated Alumina Channels for Enhanced Photoelectric Response. *ACS Nano* **2018**, *12*, 11169–11177. [[CrossRef](#)]
42. Zhang, D.; Wang, Q.; Fan, X.; Zhang, M.; Zhai, J.; Jiang, L. An Effective Dark-Vis-UV Ternary Biomimetic Switching Based on N3/Spiropyran-Modified Nanochannels. *Adv. Mater.* **2018**, *30*, e1804862. [[CrossRef](#)]
43. Xu, A.; Tang, Y.; Lin, W. Development of a mitochondrial-targeted two-photon fluorescence turn-on probe for formaldehyde and its bio-imaging applications in living cells and tissues. *New J. Chem.* **2018**, *42*, 8325–8329. [[CrossRef](#)]
44. Montoya, L.A.; Pluth, M.D. Selective turn-on fluorescent probes for imaging hydrogen sulfide in living cells. *Chem. Commun.* **2012**, *48*, 4767–4769. [[CrossRef](#)] [[PubMed](#)]
45. Fu, Y.J.; Yao, H.W.; Zhu, X.Y.; Guo, X.F.; Wang, H. A cell surface specific two-photon fluorescent probe for monitoring intercellular transmission of hydrogen sulfide. *Anal. Chim. Acta* **2017**, *994*, 1–9. [[CrossRef](#)]
46. Zhao, X.P.; Liu, F.F.; Hu, W.C.; Younis, M.R.; Wang, C.; Xia, X.H. Biomimetic Nanochannel-Ionchannel Hybrid for Ultrasensitive and Label-Free Detection of MicroRNA in Cells. *Anal. Chem.* **2019**, *91*, 3582–3589. [[CrossRef](#)] [[PubMed](#)]
47. Xia, X.; Li, H.; Zhou, G.; Ge, L.; Li, F. In situ growth of nano-gold on anodized aluminum oxide with tandem nanozyme activities towards sensitive electrochemical nanochannel sensing. *Analyst* **2020**, *145*, 6617–6624. [[CrossRef](#)]